PHILOSOPHICAL TRANSACTIONS B

rstb.royalsocietypublishing.org

Opinion piece

Cite this article: Ugurbil K. 2016 What is feasible with imaging human brain function and connectivity using functional magnetic resonance imaging. *Phil. Trans. R. Soc. B* **371**: 20150361.
http://dx.doi.org/10.1098/rstb.2015.0361

Accepted: 11 July 2016

One contribution of 15 to a Theo Murphy meeting issue 'Interpreting BOLD: a dialogue between cognitive and cellular neuroscience'.

Subject Areas:
neuroscience

Keywords:
neurovascular, brain, functional imaging, cortical layers, cortical column, resting state

Author for correspondence:
Kamil Ugurbil
e-mail: ugurb001@umn.edu

THE ROYAL SOCIETY PUBLISHING

What is feasible with imaging human brain function and connectivity using functional magnetic resonance imaging

Kamil Ugurbil

Center for Magnetic Resonance Research (CMRR), University of Minnesota Medical School, Minneapolis, MN 55455, USA

KU, 0000-0002-8475-9334

When we consider all of the methods we employ to detect brain function, from electrophysiology to optical techniques to functional magnetic resonance imaging (fMRI), we do not really have a 'golden technique' that meets all of the needs for studying the brain. We have methods, each of which has significant limitations but provide often complimentary information. Clearly, there are many questions that need to be answered about fMRI, which unlike other methods, allows us to study the human brain. However, there are also extraordinary accomplishments or demonstration of the feasibility of reaching new and previously unexpected scales of function in the human brain. This article reviews some of the work we have pursued, often with extensive collaborations with other co-workers, towards understanding the underlying mechanisms of the methodology, defining its limitations, and developing solutions to advance it. No doubt, our knowledge of human brain function has vastly expanded since the introduction of fMRI. However, methods and instrumentation in this dynamic field have evolved to a state that discoveries about the human brain based on fMRI principles, together with information garnered at a much finer spatial and temporal scale through other methods, are poised to significantly accelerate in the next decade.

This article is part of the themed issue 'Interpreting BOLD: a dialogue between cognitive and cellular neuroscience'.

1. Introduction

Almost two and a half decades after the introduction of functional imaging of brain activity by magnetic resonance (i.e. fMRI) [1,2], the neuroscience community vacillates between euphoria and scepticism about the impact of fMRI in understanding brain function and dysfunction, while the use of the technique increases by leaps and bounds. The Royal Society sponsored symposium on 'Interpreting BOLD: a dialogue between cognitive and cellular neuroscience' on 28–29 January 2016 at Chicheley Hall contained not only the presentation of the exciting uses of the methodology but also discussions on the limitations of and misgivings about the utility of the approach to the extent that the vast number of accomplishments enabled by this methodology were at the end overshadowed. Discussions of the limitations of a technique and ways to improve it are a natural and continuous process in the lifetime of any methodology. However, slightly more than two decades into the discovery of fMRI, criticism of the fMRI technique is prevalent in some corners of the neuroscience community. Sometimes, the criticism is dismissive of the fMRI method as if the other approaches employed in brain research, such as electrophysiological recordings and multi-photon based microscopy techniques, have no major limitations. Electrophysiology and photon-based techniques have highly restricted fields-of-view (regions that they can sample); they cannot perform whole brain studies; the spatial range over which neural activity may be pooled in electrophysiological recordings is complex and heavily biased towards the largest and most active neurons near the electrode tip; light cannot penetrate tissue that well, and temporal responses are limited with calcium reporters employed for detecting

spikes with photons, etc., just to name a few limitations without getting into gory details. At least electrophysiology has been around significantly longer than fMRI and is spoken of as the 'gold standard' at times. But it is at best a highly limited and imperfect gold standard. Electrophysiology can link the activity of a handful of neurons with behaviour and perception, which of course tells us that we are learning something about how the brain works. But in a way so can fMRI with many examples linking behaviour and/or perception to activity of voxels, and increasingly to ensembles of voxels that represent networks. Electrophysiology has millisecond temporal resolution, a critically important capability in understating brain function while fMRI lacks this temporal resolution; but fMRI gives us exquisite spatial coverage going from dimensions in the sub-millimetre scale to the whole brain, a capability which electrophysiology lacks. Surely, networks that span large distances over the brain are equally important for understanding brain function as temporal resolution, especially when it comes to the study of the human brain where the non-invasive nature of fMRI (unlike electrophysiology) provides an unmatched advantage.

I emphasize the afore listed limitations only to make the obvious point that we do not really have a 'golden technique' that meets all of the needs for studying the brain; rather, we have an armamentarium of techniques with their advantages and significant disadvantages. Obviously, we need to use these techniques judiciously, recognizing their limitations, while we continue to improve them to overcome their limitations. These points are self-evident. Nevertheless, the neuroscience community agonizes about the limitations of fMRI while limitations of other major techniques employed in neuroscientific research are rarely discussed. Possibly, we recognize the shortcomings of methods like electrophysiology and multi-photon techniques for the task at hand but have more confidence in the information content of the measurements themselves.

In fMRI (or in positron emission tomography (PET)), the indirect nature of the functional imaging mechanism and the uncertainties about the intermediary processes involved in neuronal activity and functional mapping signals create an easy opportunity for criticism, as well as for generating erroneous results. This has not been helped by the simplicity of obtaining fMRI data using automated, push-button data analysis programs, without necessarily paying attention to the complexities of the underlying mechanisms, without understanding the intricate implications of the imaging physics involved, and most of all, without understanding or accounting for the implications of the assumptions that go into the analysis of the data (e.g. [3] and references therein). Such studies have sometimes produced irreproducible and contradictory results, adding to the scepticism about the technique, especially when there is an easy culprit to blame, namely, the indirect coupling between fMRI signals and neuronal activity. However, the scepticism expressed often does not recognize what has been learned about this indirect coupling and what can indeed be solidly inferred from the 'indirect' activity maps provided by fMRI.

2. Improving spatial accuracy with vascular filters

In between neuronal activity and fMRI signals, we have first and foremost neurovascular/metabolic coupling. In addition, however, there is the equally important coupling between the cerebral consequences of vascular and metabolic events that accompany neuronal activity and the magnetic resonance (MR) detected signals that allow us to generate the 'functional maps'. The first is a question of physiology. The latter involves, in addition, MR physics. Both of these have been a focus in our laboratory since the introduction of fMRI. One of the first questions we tackled after the introduction of fMRI was the physiological question related to the spatial specificity of blood flow changes induced by neurovascular coupling with respect to the territorial boundaries of neuronal activity alterations. Do blood flow changes initiated by neurovascular coupling 'flood' a large patch of cortex, larger than the territory of neuronal activity changes that cause it? Or colourfully expressed, does the brain 'water the entire garden for the sake of a thirsty flower' [4,5]. This would be one way of dealing with the demands (whatever they may be, an issue still poorly understood today) of increased neuronal activity. We tackled this question by imaging quantitatively and with high spatial resolution the changes in cerebral blood flow (CBF) following stimulation of orientation columns in the cat visual cortex [6]. We were able to obtain '*single condition*' maps of orientation domains in the cat cortex by imaging the CBF changes coupled to increased neuronal activity (figure 1). It is important to emphasize that, these are *not* BOLD (blood oxygenation dependent contrast) based fMRI maps; they are images of CBF change induced by orientation selective stimuli.

Single condition means that the stimulus is contrasted against a condition lacking any of the unique characteristics of the stimulus. For example, orientation selective stimuli (e.g. a grating along a single orientation) versus a blank which has no orientation information but may have some controlling characteristics such as matched luminance; this is different from 'differential mapping' where a stimulus with one condition is contrasted against an *orthogonal* condition with the same primary features, for example, a grating with 45° orientation versus the same grating but with 135° orientation. In the latter approach, non-specific, activation-like signals that are common to the different stimuli may be suppressed, if not cancelled. The CBF data [6] showed that at the sub-millimetre scale, blood flow increased approximately 60–80%, *specifically* within the stimulated orientation domains in *single condition maps* while there was a much smaller and non-specific increase to the unstimulated cortex. Thus, our results suggested that the scenario described by the statement 'the brain waters the entire garden for the sake of a single thirsty flower' is incorrect, at least at the level of cortical columns. Rather, the brain waters the thirsty flower while it also sprinkles a large territory around it. A point-spread function (PSF) of 450 μm was calculated tangent to the cortex for the specific and large CBF increase [6]; this is in relative good agreement with recent detailed two-photon measurements [7] of neurovascular response together with imaging of synaptic and spiking activity in the cat primary visual cortex using the same orientation stimuli. The ultimate lower limit for the spatial extent of CBF regulation will depend on the location of controlling points for blood flow. Certainly, penetrating (radial) arterioles are known to exercise this control, in which case the distance between these arterioles will determine the specificity of neurovascular control of CBF relative to the neuronal activity that induces the CBF change. However, if pre-capillary and capillary control of CBF exists in addition, the territory for which 'watering' is controlled may be as little as 50 μm or so given that intercapillary distance in the brain is approximately 25 μm [8].

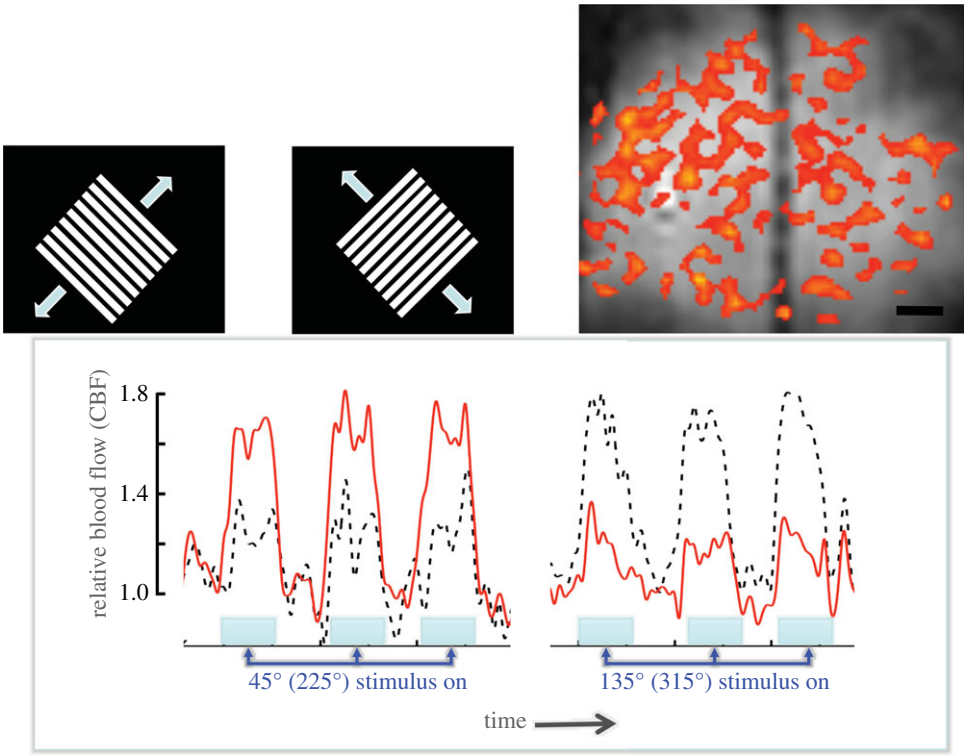

Figure 1. Single condition functional mapping of orientation columns in the cat brain using detection of cerebral blood flow (CBF) with MRI. Relative blood flow changes in response to two orthogonal grating orientations (45° and 135°) are shown. In the relative blood flow versus time plot, the blood flow changes in 'activated' versus other regions are displayed in solid red and dashed grey/black curves, respectively for the 45° stimulus, and vise versa for the 135° stimulus. Colour image shows an image obtained by thresholding based on blood flow change to suppress the regions showing the lower response for one orientation. Adapted from [6].

Thus, at least at the level of orientation columns, neurovascular coupling is specific enough to permit the mapping of such small ensembles of neurons by imaging CBF changes (ΔCBF) induced by neuronal activity. However, there is a critical methodological issue that accounts for the success of these results. When blood flow increases in a volume of tissue, it does not just magically appear there. It is delivered by larger arterial blood vessels into the capillaries where water molecules exchange between blood and tissue through the capillary walls. Blood flow must also increase in these large arteries supplying blood, as well as in the large veins draining the tissue. The blood flow increases associated with these large vessels should be contributing to any image that maps elevation in CBF. Furthermore, such large-vessel contributions to the ΔCBF images should represent an *inaccurate* component with respect to the territory of neuronal activity perturbations that induced the CBF change, extending possibly over tens of millimetres beyond the small region of activated orientation domains. Why is this 'brain versus blood vessel' confound not present in these *single condition* CBF images of activation? It is because in pulsed spin-labelling MR techniques for CBF mapping, as employed in [6], a sufficiently long delay between the spin tagging (for flow) and image acquisition suppresses signals detected from the fast flowing large blood vessels in ΔCBF maps while the technique becomes sensitive to the slower process of water molecules delivered to capillaries and exchange across the capillary wall to 'perfuse' the tissue. We had previously conducted experiments, which demonstrated that delay times longer than 1 s and approaching 1.5–2 s would be necessary to achieve this [9], and the use of such long delays was feasible at the very high magnetic field of 9.4 tesla (T) where the cat orientation domain mapping [6] was carried out.

In other words, the MR technique employed for mapping orientation domains through ΔCBF had a 'vascular filter'. Even though blood flow changes occurred in large and small (capillary level) blood vessels, the MR measurement was selectively sensitive to the latter. By contrast, the *single condition* optical imaging of intrinsic signals [10], monitoring CBV changes induced by neurovascular coupling, was shown to contain large and non-local CBV responses originating from the macrovasculature, running tangentially to the cortical sheet; differential mapping was necessary to suppress this non-specific large-vessel confound and obtain accurate depiction of the orientation columns [11]. Such optical techniques do not have the option of imposing a 'vascular filter' through the physics of the measurement as MR based ΔCBF imaging. However, they do provide high sensitivity and relatively high temporal resolution; these properties were employed to impose a 'temporal filter' by looking at the early part of the response to a stimuli (the 'initial dip') before these changes propagated to less localized and distant components [12]. These local changes were interpreted as changes in increased deoxyhaemoglobin content due to the rapidly increasing oxygen consumption rate before the onset of the blood flow response due to neurovascular coupling [12], though this interpretation remains debated (e.g. [13]).

ΔCBF based fMRI, however, is not a technique of choice for cognitive neuroscience studies in humans, especially when high spatial resolution is desired. This is because the signal-to-noise ratio (SNR) of the technique is relatively low. While anaesthetized animals can be imaged for prolonged periods to increase the SNR by averaging, similarly long experiments are not feasible in humans. Cognitive studies with humans use the BOLD-based fMRI technique [1,2], which is more complex. However, just like the CBF response detected by MR, 'vascular filters' are also needed for the BOLD approach if one is to obtain

spatially accurate functional maps with territorial fidelity to the site of neuronal activity inducing the MR signal changes.

Virtually, all cognitive studies that rely on fMRI employ gradient-recalled echo (GE) to generate the functional mapping contrast followed by echo planar imaging (EPI) to perform the image encoding; this is often referred to as GE BOLD fMRI, or just BOLD fMRI. It contains numerous contributions to the functional mapping signals (e.g. see [14] and references therein), though the BOLD mechanism is the dominant contribution under most circumstances, especially at high magnetic fields. In particular, early studies performed as single slice experiments reflected largely the inflow effects coming from fast flowing large arteries (the kind we suppressed in the CBF based orientation domain imaging shown in figure 1), leading to mapping not of focal activation but essentially angiography like images of vasculature [15]. The BOLD effect [16,17] reflects deoxyhaemoglobin (dHb) content in the brain, which is determined by CBF, CBV and the cerebral oxygen consumption rate ($CMRO_2$). Upon an increase in neuronal activity, CBF increases regionally as a result of neurovascular coupling but $CMRO_2$ is not elevated commensurately (e.g. [18] and references therein); consequently, the dHb concentration in blood decreases in the region where these CBF changes take place. Despite an increase in CBV, the dHb content per unit volume of brain decreases also. But the dHb concentration changes in blood do not remain stationary in space; they propagate down the draining veins and show up in regions distant from the tissue where neuronal activity was altered. Ultimately, it is diluted in distant veins due to pooling of blood from regions where neuronal activity was unperturbed. This 'draining vein' problem in GE BOLD fMRI was experimentally seen and reported very early in the development of fMRI [19–22]; the problem was visited with modelling several years later, coming to the conclusion that there could be changes in venous blood detectable as apparent 'activation' as much as 4 mm beyond the edge of a 100 mm^2 activated area [23]. These numbers are also consistent with a PSF of approximately 3.5 mm reported for GE BOLD fMRI at 1.5 [24] and 3 T [25]. An inaccuracy of approximately 4 mm does not seem like much of a problem; after all, in many human fMRI studies, the effective spatial resolution dictated by image acquisition is intrinsically not much better than approximately 4 mm. However, in the convoluted human brain, approximately 4 mm accuracy can actually represent a major confound. Two banks of a sulcus can be physically very close and can show apparent activation on both banks due to draining pial vessels in the sulcus, but they are likely to be miles apart functionally, performing completely different tasks. It is also a major limitation when highly granular functional mapping, such as mapping of columns and layers are desired (see below).

Thus, GE BOLD fMRI has a 'draining vein' problem, just like CBF fMRI has a large blood vessel problem. One can predict that GE fMRI should not be able to generate functional maps of orientation columns as shown in figure 1, and this is what is observed experimentally (figure 2): when functional imaging with GE BOLD is performed in the same visual areas of the cat as in figure 1 and with the same stimuli, four different orientations of the stimulus result in virtually the same map, with the highest changes detected in the sagittal sinus running in the interhemispheric fissure (figure 2). Thus, a 'vascular filter' is also needed for BOLD fMRI.

For BOLD-fMRI, we pursued imposing a "vascular filter" on the acquisition of functional maps through the use of

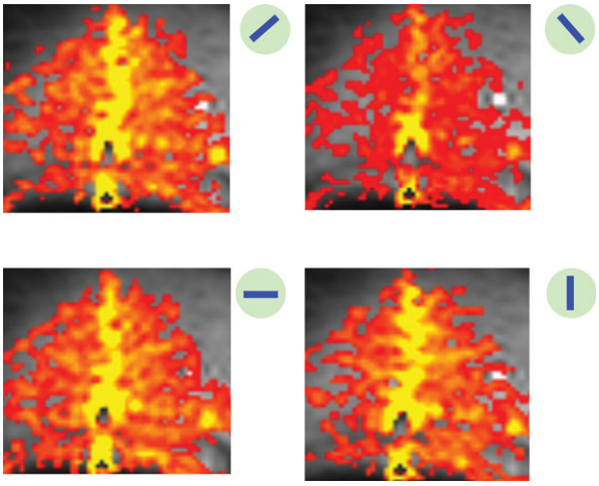

Figure 2. As in figure 1, but images obtained with gradient echo BOLD fMRI for four different orientations of the stimulus.

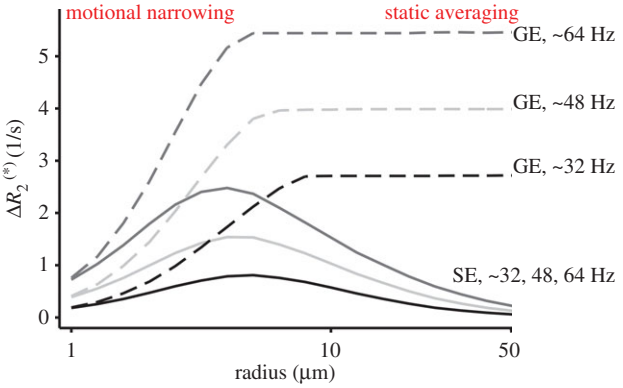

Figure 3. Extravascular relaxation rate changes for R_2 and R_2* (equal to $1/T_2$, and $1/T_2$*, respectively) induced by simulated blood vessels with a magnetic susceptibility difference between blood vessel interior and exterior (basis of extravascular BOLD effect), shown as a function of blood vessel radius and magnetic susceptibility induced different frequency shifts (in Hz) across the blood vessel. The numbers 32, 48 and 64 Hz correspond to increasing magnetic field strength B_0 at a constant deoxyhaemoglobin concentration (approx. 3, 5, and 7 T at physiological venous deoxyhemoglobin levels) or increasing deoxyhaemoglobin concentration at a constant B_0. GE, gradient echo; SE, spin echo. From Uludag & Ugurbil [28].

spin echoes instead of the conventional gradient echoes; this strategy was motivated by the modelling predictions published first in 1993 [26] and later expanded considerably by us and others ([14] and references therein). Spin echo fMRI signal characteristics differ significantly from GE fMRI (e.g. [27]) (figure 3). However, there exist fine but important mechanistic and implementation points about SE fMRI that are often overlooked. SE fMRI selectivity for small diameter blood vessels (figure 3) is true for *extravascular* BOLD effect; in other words, the BOLD effect associated with magnetic field inhomogeneities induced in tissue outside of a blood vessel containing dHb. But, there is also an 'intravascular' effect associated with apparent T_2 changes of blood itself caused by neuronal activity alterations through neurovascular coupling (e.g. [14,29–32] and references therein). The intravascular effect is not subject to vascular selectivity by SE fMRI *per se*, and appears in all sections of the vasculature where dHb concentration is altered due to neuronal activity in some part of the brain. Thus, draining veins should show up in GE- or SE-based functional images due to such an

intravascular effect as far away as approximately 4 mm [23] from the actual site of neuronal activity changes. However, this non-specific 'intravascular' component is dramatically suppressed with increasing magnetic fields. The MR detectability of dHb containing blood decreases precipitously with increasing magnetic fields. Therefore, if the dHb containing blood is absent in an MR image to begin with, such intravascular effects related to neuronal activity changes would also not be detected; this happens at very high magnetic fields (7 T and above) when the echo times (TEs) employed are long compared with blood T_2 at the magnetic field used [29].

In other words, the *vascular filter* of SE fMRI is very much dependent on magnetic field magnitude. However, the very high magnetic field by itself is not enough; one must in addition make sure the TE in the SE sequence is long compared with the T_2 of dHb containing blood. Fortuitously, while the T_2 of dHb containing venous blood and the T_2 of tissue both decrease with increasing magnetic fields ([14,29] and references therein), the former decreases much more rapidly. Therefore, at 7 T and above, T_2 of tissue becomes much longer than blood T_2 [29]. Thus, if one chooses the TE to be approximately equal to tissue T_2 at 7 T or higher magnetic fields (which would be the optimum for detecting SE functional imaging signals in high-resolution fMRI (e.g. see fig. 8.7 in [28])), dHb containing blood would be suppressed while the functional imaging signals associated with tissue due to extravascular BOLD would be optimized. Sometimes, for a variety of reasons, such a TE is not quite feasible or is not chosen; then, even at 7 T or much higher magnetic fields one can still get this undesirable intravascular contribution to SE fMRI images. At 4 T, for example, choosing a TE of 32 ms results in intravascular blood contributing approximately 80% of the 'functional' signals detected by SE fMRI, whereas a TE of 65 ms yields a contribution of approximately 20% intravascular BOLD (see Fig. 3 in [29]). One cannot keep increasing the TE *ad infinitum*, however, with the hope of suppressing the blood effect, because tissue signals also start decreasing when TE exceeds tissue T_2, thus diminishing the likelihood of detecting any functional signals. At 7 T and above, however, the difference between dHb containing blood and tissue T_2 is such that one can suppress or even eliminate the former while optimizing the latter. This is not possible at 3 T [25,33] or even 4 T [29] because at reasonable TE values approximating tissue T_2, the intravascular BOLD contribution remains a major component of the SE fMRI signals. These have been predicted by numerous other modelling efforts and are reviewed in [14,28].

Intravascular effects can also be suppressed using diffusion weighting gradients. However, this also introduces potential confounds, especially in the presence head motion; as such, they are not necessarily a desirable approach except for studies examining the mechanisms and the source of functional mapping signals (e.g. [29,34]).

Finally, there is an implementation problem with SE fMRI. Some GE BOLD characteristics can appear because of the imaging sequence, particularly with EPI or spiral based rapid single shot imaging sequences preferred in functional imaging studies. In such sequences, there is only a single point in k-space (i.e. a single time point in the acquired data) that meets the full spin echo condition. All other points in the data also have some gradient echo weighting. Thus, in the most commonly used EPI approach, the echo train lengths have to be kept short using approaches such as segmentation, highly parallel imaging along the phase encoding direction, and partial Fourier acquisitions. Otherwise, the spatially non-specific contributions masquerading as functional maps appear even in SE based functional images (e.g. [35]).

Recently, an alternative approach was described exploiting the fact that the majority of the undesirable large-vessel signals associated with the GE BOLD effect (signals that obfuscate the true territory of neuronal activity change) are the pial vessels located on the cortical surface. So, if fMRI data are acquired at high enough resolution (possible at very high magnetic fields), then some fraction of the upper cortical layers can be stripped away and the functional mapping analysis restricted to the remaining deeper layers of the cortex [36]. Using retinotopy as a source of stimulation, these investigators were able to show that they obtained accurate depiction of the stimulus in the brain when looking selectively at deeper layers but not the superficial layers [36]. Note that one cannot just strip off the anatomical space occupied by the blood vessel itself because the extravascular BOLD effect is associated with the tissue space outside the vessel boundaries and significantly penetrates into the space surrounding the blood vessel. Therefore, one must strip away some of the superficial cortical layers for this analysis. Recently, this approach was used to map colour- and disparity-selective columns within the human visual system [37].

Eliminating the superficial cortical layers to suppress the false activation associated with pial vessels is a 'vascular filter' applied based on the spatial location of the blood vessels. Just like SE fMRI, however, it also leads to a decrease in the total fMRI signal because the pial vein component of the fMRI signal, which is also the larger component, is discarded. This approach also differs from SE fMRI in other aspects; superficial cortical layers are eliminated from the analysis, and as such, layer-dependent fMRI examining the role of upper cortical laminae (e.g. [38–40]) is not feasible. In addition, the intracortical radial blood vessels are not suppressed by this approach but would be suppressed by the SE approach. This may also impact layer-dependent fMRI.

Exploiting the time course of the evolution of the neurovascular response to improve accuracy has also been pursued in fMRI studies in the human brain; the 'initial dip' first reported in optical studies was also observed in numerous human fMRI studies (e.g. see review [41] and references there in) largely coming from our group. However, we ultimately abandoned this approach as a means of reaching the resolution of columns and layers in the human brain, not because it lacks spatial fidelity, but because it is a small effect and simply does not have the sensitivity as an fMRI method to provide high-resolution imaging in the human brain.

3. Functional contrast-to-noise ratio

The SE fMRI approach is sometimes criticized because functional mapping signals are small; but this is the price one pays for improved spatial accuracy. The loss can be made up by using high magnetic fields. In fact, SE fMRI at 7 T has roughly the same functional signal change, and probably a better functional contrast-to-noise ratio (fCNR), as GE BOLD fMRI at 3 T.

Taking into account what is known about the neurovascular coupling induced physiological changes, the SE fractional signal changes ($\Delta S/S$) expected in the brain in response to

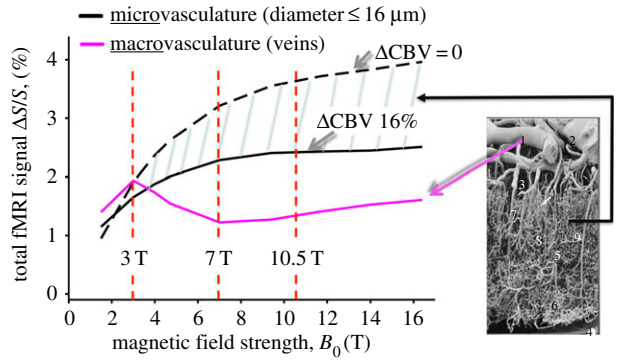

Figure 4. Simulation of spin echo (SE) detected fractional signal changes ($\Delta S/S$) induced by neuronal activity at TE = tissue T_2. Physiological parameters used: for microvasculature: Microvascular CBV = 2.5%, composed of 20% arteriole ($d = 16$ µ), 40% capillary ($d = 5$ µ), and 40% venule ($d = 16$ µ). ΔCBV is taken as either as 0 or 16% in all. For macrovasculature vessels: CBV = 5%; diameter, $d = 200$ µ; 90° to B_0 (worst case scenario); ΔCBV = 0; a larger ΔCBV would reduce the contribution coming from this component. Adapted from Uludag *et al.* [14].

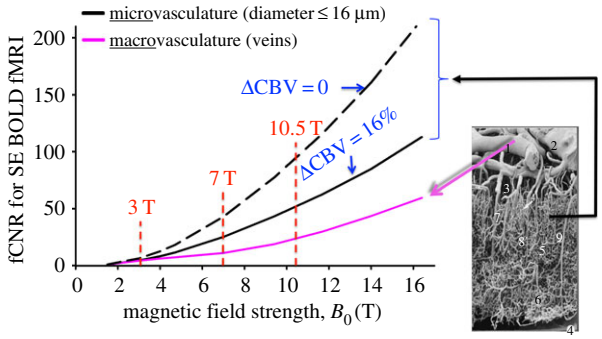

Figure 5. Functional contrast-to-noise ratio (fCNR) for SE BOLD fMRI will be proportional to the curves shown, which are obtained by multiplying $\Delta S/S$ in figure 4 with $B_0^{1.65}$, normalized to the value at 1.5 T. These plots are valid only in the limit the noise in the fMRI time series is dominated by thermal noise of the image, which is the case, for example, for high-resolution imaging at the level of cortical columns and layers. Plots generated by Uludağ K using data from Uludağ *et al.* [14].

alterations in neuronal activity were calculated [14]; the data from this paper are adapted and are shown in figure 4. These simulations are different to those shown in figure 3, which serve as a starting point; then neuronal activity induced intravascular effects, relevant physiological and anatomical parameters about the brain and the neurovascular coupling, and NMR parameters are all taken into account in order to estimate the *total* fractional signal change expected from an fMRI experiment (see figure 4 legend for some of the parameters included in the simulation). For microvasculature, ΔCBV coupled to neuronal activity was taken either as 0 or 16%, the range of values reported for CBV change in general. The magnitude of the capillary CBV changes due to neurovascular coupling is controversial (e.g. [42–45]); a recent optical imaging study indicated that capillary diameter changes in the cat visual cortex are small (beyond the detection of the microscopy technique employed or non-existent) [7]. Hence, the ΔCBV = 0 curve may be the appropriate curve to consider for capillaries. Also, the 'macrovascular' contribution shown here would not be applicable to all image voxels; it would only be present when a large blood vessel is present in the voxel and has a 90° orientation to the main magnetic field (the scenario that was considered, which is the worst case scenario); a large-vessel running parallel to the static magnetic field would have no contribution. For the macrovascular effect, vessel diameter would not come into play in the BOLD effect *per se* (figure 3) but the blood volume occupied by the large blood vessel in the voxel would impact the magnitude of this contribution. The results of the simulation shown in figure 4 were consistent with experimental data (discussed in [14]). Very similar results were also obtained using a realistic model of the vasculature obtained with two-photon microscopy [46].

The achievable spatial resolution and/or the accuracy of the imaging measurements are determined by the contrast-to-noise ratio. In BOLD fMRI, the contrast-to-noise ratio for functional mapping, i.e. *functional contrast-to-noise ratio* or fCNR, can be written as

$$\mathrm{fCNR} = \frac{\Delta S}{N_t} = \left(\frac{\Delta S}{S}\right) \cdot \left(\frac{S}{N_t}\right) = \left(\frac{\Delta S}{S}\right) \cdot \left(\frac{(\alpha S_0 \cdot \mathrm{e}^{-\mathrm{TE}/T_2^X})}{N_t}\right). \quad (3.1)$$

In this equation, ΔS is the stimulus or task induced signal change, N_t is the temporal signal fluctuations in an fMRI time series, and S is the steady-state signal amplitude for a given voxel in the image detected in the fMRI time series in the absence of the stimulus (but note that $\Delta S \ll S$, so the caveat that this is in the absence of the stimulus does not matter so much), and S_0 is the thermal equilibrium magnetization. The signal amplitude S depends on the flip angle (FA) of the excitation pulse, the repetition time (TR) in the fMRI time series, and the longitudinal relaxation time T_1, as well as on the delay TE employed after the excitation pulse to generate the BOLD contrast. During the TE, the signal decays exponentially with time constant T_2^X, which designates either T_2 or T_2^* (for spin echo or gradient echo, respectively) depending on the type of contrast employed to generate the functional signals. The FA, TR and T_1 effect can be expressed in terms of the thermal equilibrium magnetization S_0 and a constant α, which varies between 0 and 1; α accounts for the saturation effect and approaches 1 when the TR is sufficiently long compared to T_1 to allow full relaxation for the FA employed.

For an fMRI time series, $N_t \geq N_{\mathrm{thermal}}$ [47–50], where N_{thermal} designates the 'thermal' noise of the image; at high spatial resolutions, however, $N_t \sim N_{\mathrm{thermal}}$, leading to

$$\mathrm{fCNR} = \frac{\Delta S}{N_{\mathrm{thermal}}} = \left(\frac{\Delta S}{S}\right) \cdot \alpha[\mathrm{SNR}_{\mathrm{image}}]\, \mathrm{e}^{-\mathrm{TE}/T_2^X}, \quad (3.2)$$

where $\mathrm{SNR}_{\mathrm{image}} = \dfrac{S_0}{N_{\mathrm{thermal}}}$. We had experimentally documented that $\mathrm{SNR}_{\mathrm{image}}$ increases slightly more than linearly with B_0 in going from 4 to 7 T [51,52]; recently, $\mathrm{SNR}_{\mathrm{image}}$ was reported to scale as $B_0^{1.65}$ based on experimental data obtained over the range 3 to approximately 10 T with multichannel array coils [53]. For SE contrast, taking $\Delta S/S$ as the data shown in figure 4 and multiplying with $B_0^{1.65}$ dependence of $\mathrm{SNR}_{\mathrm{image}}$ yields a dramatic supralinear gain in fCNR (figure 5). The same would also be true for fCNR for GE BOLD (figure 6) based on increases in $\mathrm{SNR}_{\mathrm{image}}$ and $\Delta S/S$ [14,54].

4. High-resolution functional mapping

Thus, particularly for high-resolution BOLD fMRI, increasing magnetic fields provide multiplicative gains: significant

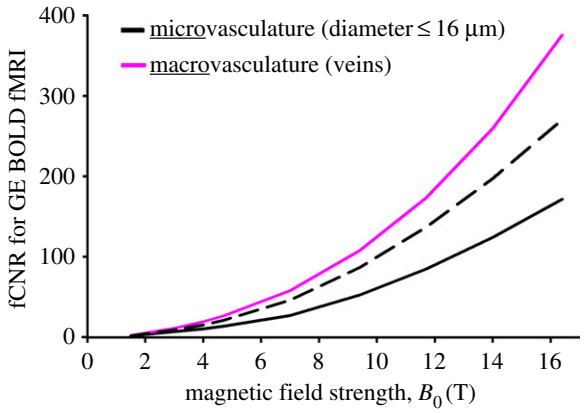

Figure 6. Functional contrast-to-noise ratio (fCNR) for GE BOLD fMRI. As in figure 5 but calculated using $\Delta S/S$ for GE BOLD fMRI data from Uludağ *et al.* [14]. Microvascular contribution is calculated with $\Delta CBV = 0\%$ (dashed line) or 16% (solid line), as in figure 5.

improvements in fCNR that can be traded for spatial resolution and/or for better quantification, and increased contributions from the microvascular mediated mapping signals that could allow functional mapping at the level of small functional ensembles such as cortical columns and layers. This is the reason why we launched the development of 7 T in the mid-1990s, achieving operational state in approximately 1999 [55]. This 'lego' MR system was assembled and integrated by CMRR scientists from parts acquired from different suppliers or built within CMRR, using the first 7 T/90 cm bore magnet developed by Magnex Scientific in a collaborative effort they undertook with us [55]; as such, this instrument did not have the research and development (R&D) engineering that exists behind today's commercially available scanners. Nevertheless, the feasibility of anatomical imaging at such a high field and SNR gains with increasing field strength (at the time a hotly debated topic) [51] were demonstrated. Additionally, superior fMRI performance compared to 4 T was observed as predicted from our understanding of mechanisms underlying MR based functional maps [54]. The ultimate goal for pursuing this high magnetic field was to reach spatial resolutions and precision where one can obtain functional maps of computational ensembles of neurons that process highly reduced features of a stimulus or a task. We used the ocular dominance and orientations columns as the test bed and finally, using SE fMRI and 7 T, robust maps of orientations columns together with ODCs in the same subjects were achieved [56] (figure 7). In the orientation maps, the boundaries of the ODCs are shown as dark lines (figure 7). The expanded orientation figure shows many features of the orientation maps that have been known from animal model studies, namely the pinwheel centres (white circles) around which the orientation representation runs either clockwise or anticlockwise, the pinwheel centres appearing predominantly in the centre of the ODCs, and the linear zones of a preferred orientation running approximately orthogonal to the ODC boundaries. It is important to emphasize that the increasing contribution that comes from microvasculature at 7 T (figure 4), the ability to suppress the extra- and intravascular large-vessel confound using spin echoes and 7 T together, and the increasing intrinsic image SNR underlie the success of this result.

Although the above data were obtained with SE fMRI, some success can be had in such fine scale mapping with GE fMRI if one avoids regions with large vessels [57,58]. Figure 8 shows *reproducibility* of SE and GE fMRI maps of ODC on the same subject for two different days [58]. They are both highly reproducible, preserving the pattern of one eye versus the other extremely well except in the transition zones where reproducibility is expected to be poor due to partial volume effects. However, these maps also show that while in the GE images there are regions where the ODC pattern is observed, in other areas (identified by the dashed white line) the ODC pattern is not present, presumably due to the large-vessel confound.

With the introduction of commercial 7 T instruments, increasingly we have seen this ultrahigh field used for attaining improved fCNR, spatial resolution, and fidelity to sites of neuronal activity in BOLD fMRI in the human brain at the level of cortical layers, either demonstrating and/or examining layer specific functional signals (e.g. [34,36,59–62]) or using this capability to investigate laminar specific computations [38,40,63], cortical columns [37,40,56,58,59], and other fine scale organizations, such as the digits of the hand [64–66], and tonotopy in the inferior colliculus (IC) [67,68] and medial geniculate body (MGB) [67]. The high field advantages have also been covered in several different review articles (e.g. [28,69–77]).

Figure 9 displays a composite figure that summarizes accomplishments with 7 T we in CMRR have undertaken in collaboration with colleagues in Maastricht University since 7 T became operational in CMRR. It also illustrates the evolution of ultrahigh field fMRI, and what is now feasible with this technology. The very first 7 T study was the tonotopic mapping in the human auditory cortex [78]. At the time, the existence of mirror-symmetric tonotopic maps were known from animal model studies but were not achieved in the human brain. The 7 T work showed the first mirror-symmetric maps in the human brain, and also demonstrated extremely high reproducibility of the data [78]. The functional organization of human auditory subcortical structures were only inferred from animal models until the organization of spectral responses was mapped for the first time at 7 T in the human IC, a small, approximately $7 \times 7 \times 7\ mm^3$ subcortical structure fundamental for sound processing. In 2015, 7 T was used again to investigate auditory processing in another subcortical structure in the human brain, the MGB [67], a smaller structure than the IC, with dimensions of approximately $4 \times 5 \times 4.5\ mm^3$; the study showed that two tonotopic maps characterized the MGB, reflecting its two subdivisions [67]. More recently, going back to the human primary auditory cortex, high-resolution fMRI experiments at 7 T provided evidence for the columnar organization of the processing of sound frequency and showed that frequency preference is stable through cortical depth [40]. Furthermore, in this highly columnar cortex, the fMRI data with laminar resolution revealed that task demands sharpen the frequency tuning in superficial cortical layers more than in middle or deep layers [40].

The afore listed auditory studies were conducted using tones as well as natural sounds, the later using encoding methods similar to the approach introduced for the study of the visual cortex [79,80]. Some of these studies used both 3 T and 7 T data and different models for the processing of sounds in the human brain. For each model, however, 7 T data performed significantly better than the 3 T data [81]. The cause of this is probably not only the increased SNR and fCNR at the higher field strength but also the fact that at these high fields there is higher granularity to the information content detected in fMRI; in other words,

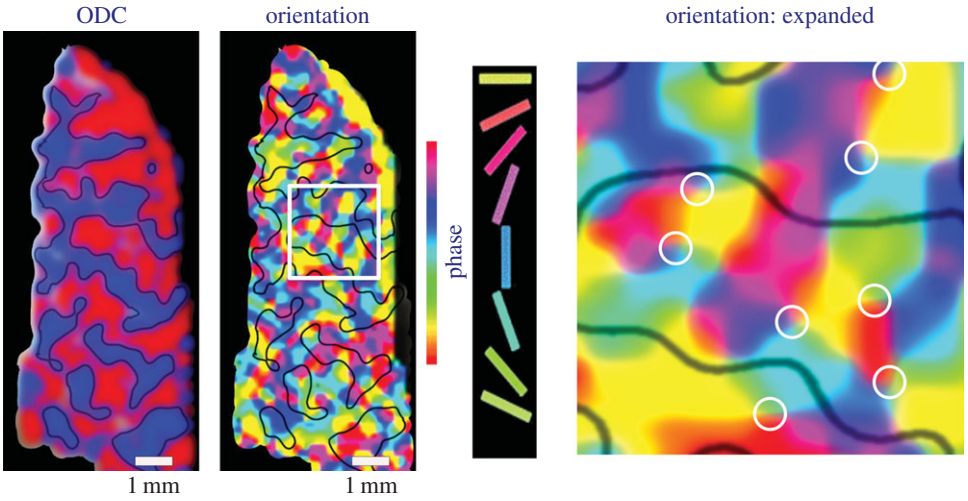

Figure 7. Functional maps of orientation and ocular dominance columns in the human brain. Obtained at 7 T using SE fMRI. Adopted from Yacoub *et al.* [56].

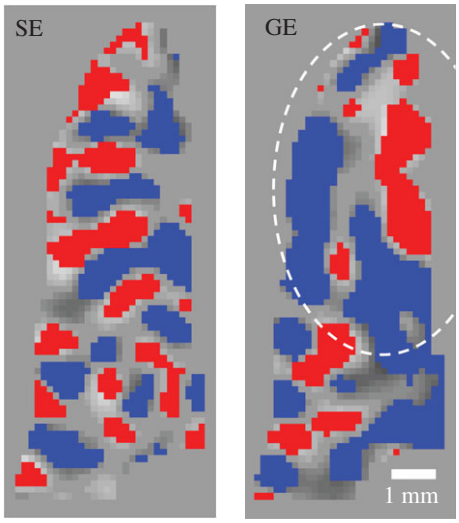

Figure 8. Ocular dominance column functional images obtained either by spin echo (SE) or gradient echo (GE) fMRI on two separate occasions on the same individual. Each voxel is labelled with either blue or red colour if it is *reproducibly* assigned to the same eye on the two different occasions. Thus, the maps shown depict the patterns induced by stimulation of one eye *versus* the other, as well as their reproducibility in a single subject on two different occasions. Adapted from Yacoub *et al.* [58].

distinctly different functional information content that is organized at a much finer spatial scale, such as cortical columns and layers, can be detected and distinguished in adjacent voxels. At lower fields, when the capillary contributions are weak and the fMRI data are dominated by effects originating from large blood vessels, many adjacent voxels are expected to be highly correlated no matter how high the intrinsic resolution of the images are. However, at 7 T and beyond, increasingly each voxel begins to display independent information even at very high resolution. Ultimately, the purpose of such high resolution and high fidelity mapping is that, when such granularity of computation exists in the brain, we need to incorporate it in models of information processing in the brain. In this respect, the ultrahigh field studies hold major advantages and the auditory cortex work referenced above and similar work conducted on the visual system at 7 T [82] provides examples of significant improvements.

With the drive towards significantly higher magnetic fields than 7 T and SNR enhancing technologies, such as RF coils with a large number of small coil elements forming a dense array (which tend to work better at very high magnetic fields) and the use of unique dielectric materials, it is interesting to speculate how one may expect to perform very high-resolution fMRI in the near future. $\Delta S/S$ for SE fMRI plateaus after about 10 T and the gains would come predominantly from intrinsic image SNR. But GE fMRI would continue to benefit from increases in both image SNR and $\Delta S/S$, albeit carrying with it the large-vessel confound. *However, in the limit of very high resolution* (provided such high resolutions can be reached), GE fMRI maps would be like optical imaging maps where we would clearly see the ODC or orientation domains with some large-vessel signals running through the maps but predominantly confined to the vessel boundaries. Previously, it was mentioned that the extravascular BOLD effect penetrates into the tissue some significant distance away from the luminal boundaries of the dHb containing vessels. When the resolution becomes very high and voxel size is small, however, this effect would approach the limit where intravoxel inhomogeneity will be small and consequent signal loss due to dephasing of signals within the voxel will be negligible; rather than a signal loss, the BOLD effect from the large vessel would be a phase difference in the voxel. This phenomenon would not be associated with capillaries as long as the voxel size remains large compared to intercapillary distance and, consequently, the voxel contains many capillaries spanning different orientations. Such phase differences associated with large vessels have been noted before and used to identify and suppress the large-vessel effects at relatively moderate resolutions employed today [83]; however, at low resolution, phase effects induced by large vessels are also accompanied by signal loss due to the intravoxel inhomogeneity (the BOLD effect) coming from the same blood vessel and a clear separation is not completely feasible. But at very high resolutions, the signal loss associated with the large vessel would be minimized leaving only the phase effect allowing a cleaner separation of large and small vessel contributions, even close to the large-vessel boundaries.

5. Relationship to electrical activity

The relationship between the fMRI signals and local neural activity remains a topic of ongoing research and discussion. A review of this topic is beyond the scope of this article. Some

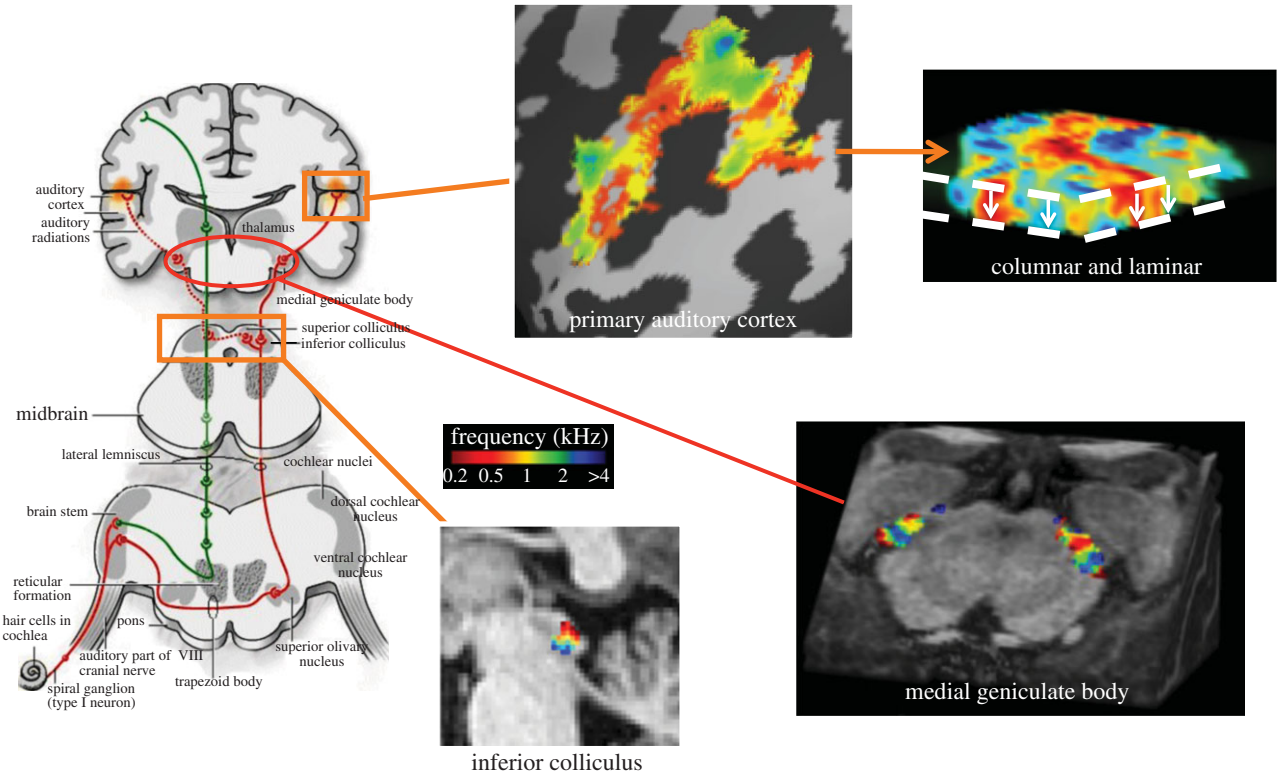

Figure 9. Mapping frequency selectivity in the auditory pathway. Adapted from Formisano *et al.* [78], De Martino *et al.* [68], Moerel *et al.* [67], and De Martino *et al.* [40].

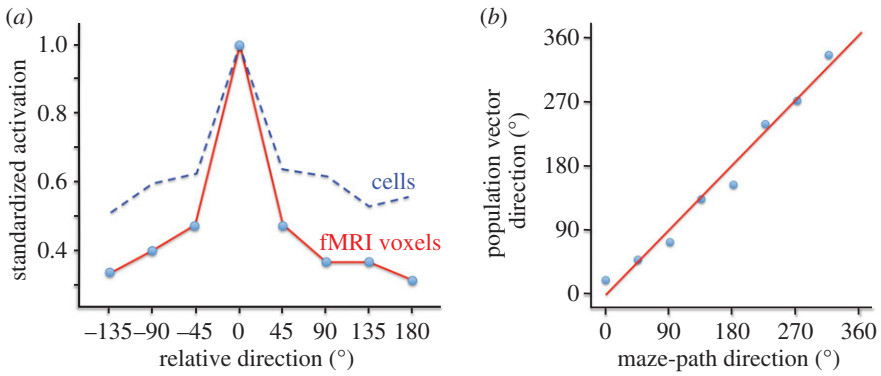

Figure 10. (*a*) Standardized population-tuning curve in the human superior parietal lobule (SPL) in a maze-path direction task shown together with the standardized population-tuning curve obtained with single cell electrophysiology recordings in the posterior parietal cortex of monkeys performing practically identical tasks. All tuning curves were standardized with respect to their range, aligned to their maximum and averaged across voxels or cells. (*b*) The correlation between the actual maze-path direction and that predicted by the population vector calculated from MR voxels. Adapted from Gourtzelidis *et al.* [87].

recently published reviews cover this topic in some detail [84]. However, numerous studies take advantage of observations that, under most circumstances, the relationship between local neural activity and the fMRI response is approximately linear. This was extended also to the negative BOLD responses observed in the human brain [85], which were shown to be associated with decreases in neuronal activity in simultaneous electrophysiology and fMRI studies in monkeys [86]. Here, data from one of our studies are presented as an example showing that fMRI voxels can provide similar information and the same link to behaviour as electrophysiology. Figure 10*a* displays the standardized population-tuning curves in the human superior parietal lobule (SPL) measured with fMRI in a maze-path direction task [87,88] and with single cell recordings in posterior parietal cortex of monkeys performing practically the identical task [89]. To obtain the general form of the tuning curve displayed in this figure, all tuning curves were standardized with respect to their range, aligned to their maximum and averaged across voxels or cells. The result was a population directional tuning curve that looks virtually identical irrespective of the method employed, fMRI in humans and single cell recordings in monkeys (figure 10*a*) [87]. What is equally important is that the population vector, calculated from the whole ensemble of directionally tuned fMRI voxels, predicted very well the direction of the maze path just as well as the cell recording (figure 10*b*).

6. Resting-state functional magnetic resonance imaging

Resting-state fMRI (rfMRI) uses correlations in the spontaneous temporal fluctuations in an fMRI time series to deduce '*functional connectivity*'; it serves as an indirect but nonetheless invaluable

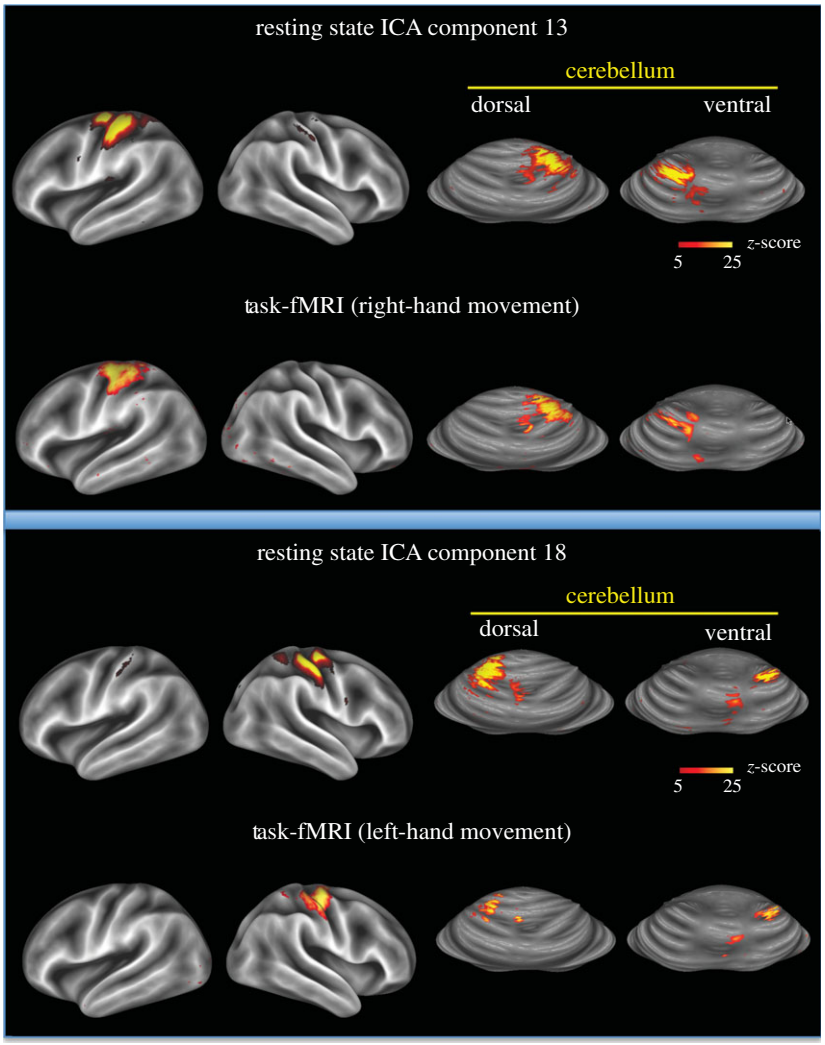

Figure 11. Comparison between activation patterns observed with task-fMRI when subjects are performing a simple 'hand task' with the right- or left-hand and ICA components extracted from the 3 T resting-state fMRI data from the Human Connectome Project (HCP) database. Patterns mapped onto the group-average inflated cerebral and the cerebellar atlas surface that has been mapped to the MNI atlas stereotaxic space. Adapted from Van Essen *et al.* [104].

indicator of grey-matter regions that interact strongly and, in many cases, are connected anatomically (e.g. [90–98]). The existence of spontaneous fluctuations in an fMRI time series and the possibility that they could yield connectivity information, provided they were found to be of neuronal origin, was first mentioned in 1993 [26], shortly after the introduction of fMRI itself in 1992. However, rfMRI came into existence when it was first reported that the fMRI time series from the motor cortices of the two different hemispheres were temporally correlated with each other in the absence of any task [90]. This observation extends beyond the motor cortex: functionally linked areas (though not necessarily all directly connected) exhibit distinct correlated spontaneous oscillations and thus can be extracted from the rfMRI data (e.g. [95]). Hence, it is possible to identify from rfMRI data the so-called resting-state networks (RSNs) that can be classified and identified such as 'visual' or 'sensory-motor', or 'language', etc., networks. The identifications are based on the observation that the spatial patterns that are depicted in these RSNs (which resemble activation maps but are actually regions that display temporally correlated spontaneous fluctuations) have similarities to collection of regions activated by task-based fMRI.

The recent Human Connectome Project (HCP) data, which is publically available (https://www.humanconnectome.org/data/), represent probably the most advanced rfMRI data at present and provides some of the best demonstration to date of this phenomenon. HCP data were acquired with highly accelerated fMRI techniques that permitted whole brain coverage in 0.7 s for 2 mm isotropic resolution [99] and subsequently cleaned up by independent component analysis (ICA) based methods [100]. These slice accelerated methods have been transformative in functional imaging as well as diffusion-weighted imaging (dMRI) that is employed for tractography analysis. In rfMRI, they have enabled the detection of significantly larger RSNs as well as improving the statistical power of the observations [98,101]. It is also critical that potential confounds that also produce spatial patterns of correlated activity (e.g. [102,103]), due to fluctuating physiological processes such as respiration and cardiac pulsation, need to be identified and removed from the data [98]; in this respect, the highly accelerated data of the HCP also provide advantages by providing a higher sampling rate for capturing these fluctuations more accurately [98]. An example of RSN's extracted by ICA analysis compared with task induced activation maps from the 3 T HCP data [104] are illustrated in figure 11. The striking similarity between the RSNs and the task induced activation provide yet another excellent example demonstrating that regions that are intimately linked functionally do have correlated spontaneous fluctuations even when they are not actively involved in the execution of a task. This conclusion also supports the position that these correlations are of neuronal origin. Of course, there has been additional data from a variety

of electrical and optical recordings, with or without the concurrent use of fMRI in animal models and in humans that support this conclusion (e.g. [105–113]) although the exact nature of the link remains a point of discussion.

Resting-state fMRI data yield many RSNs; in this regard, HCP data are unique in being able to identify a very large number of such RSNs that are spatially much more fine grained than what was previously available [97,98]. It is not immediately possible to identify an association between all of these RSNs and an activation pattern elicited with a specific task. This is expected; for example, a visuo-motor task, such as moving a joy stick in the direction of a target presented to the subject, will yield a very large number of activated areas in the brain. A single RSN that corresponds to those areas is not likely to be identified. Instead, RSNs that represent motor networks, visual networks and others (probably involving parietal areas) together will represent the task induced activation pattern. It was in fact recently shown that it is indeed possible to predict the activation patterns invoked during task performance from the resting-state data, and it is possible to do this on an *individual* basis [114].

Based on the publically released 3 T rfMRI data from the HCP, significant biological conclusions have already been published. Investigating the relationship between individual subjects' functional connectomes and 280 behavioural and demographic measures in a single holistic multivariate analysis, Smith *et al.* [115] identified one strong mode of population covariation along a single 'positive–negative' axis-linking lifestyle, demographic and psychometric measures to each other and to a specific pattern of brain connectivity. Finn *et al.* [116] demonstrated that 'functional connectivity profiles act as a 'fingerprint' that can accurately identify individual subjects from a large group'. Identification was successful across scan sessions and even between task and rest conditions, indicating that an individual's connectivity profile is intrinsic, and can be used to distinguish that individual regardless of how the brain is engaged during the imaging session. Hawrylycz *et al.* [117] examining genetic signatures of the adult human brain report that 'highly consistent transcriptional architecture in neocortex is correlated with resting-state functional connectivity, suggesting a link between conserved gene expression and functionally relevant circuitry'.

The largest publically released dataset from the HCP will be a 3 T dataset. However, in approximately 180 subjects that initially participated in the 3 T scanning, 7 T data were also acquired and are becoming publically available. Some initial results from these 7 T data sets were published for dMRI [118,119]. Preliminary analysis of the 7 T resting-state data shows significant gains in contrast-to-noise ratio and the number of ICA components that can be classified as RSNs, even though the resolution of the 7 T data is higher (1.6 mm isotropic versus 2 mm isotropic, resulting in approximately twofold smaller voxel volume at 7 T) (K Ugurbil 2016, unpublished data). Hence, it can be expected that the 7 T resting-state data will yield additional inferences about human brain function compared to the already successful 3 T data.

7. Conclusion

In the armamentarium of methods we employ to detect brain function, from electrophysiology to optical techniques to fMRI, we do not really have a 'golden technique' that meets all of the needs for studying the brain. Each method has significant limitations but often provides complimentary information. fMRI among them is the only technique that can provide rich information directly in the human brain. Clearly, it has limitations, temporal resolution in the millisecond time domain and the sluggish (and probably regionally varying) neurovascular response being the primary ones. Clearly, the link to facets of neuronal activity needs to be better defined. But it has excellent spatial fidelity and resolution when employed properly, especially at very high magnetic fields, and also provides increasingly interesting information on functional connectivity and networks. No doubt, our knowledge of human brain function has vastly expanded since the introduction of fMRI. With many new initiatives such as the HCP and the BRAIN Initiative in the USA (and similar undertakings in numerous other countries), new developments in instrumentation, methods of image acquisition, reconstruction, and analysis, and more precise inquiries into the neuronal and vascular mechanisms underlying fMRI (e.g. [7]) will accelerate. We have not by any means plateaued; much is left to accomplish without even the introduction of disruptive technologies that may one day pop up in the dynamic environment of brain imaging research, leading to transformative leaps. Efforts exploiting high magnetic fields have the potential to push fMRI to the spatial scale that overlaps with techniques like multi-photon imaging so that the activity of a collection of neurons that can be studied with fMRI at the level of the ensemble can be mapped at a single neuron level with other techniques, (figure 12) albeit not in the human brain. Such a capability requires further technological developments in fMRI, which appears realizable in the not too distant future, as well as in multi-photons imaging. Together, the approaches can provide information from single cells to the entire brain (in the same species for animal models but combining animal model studies with human experiments when the human brain is the target), and ultimately behaviour, significantly accelerating discoveries in this new century of the brain.

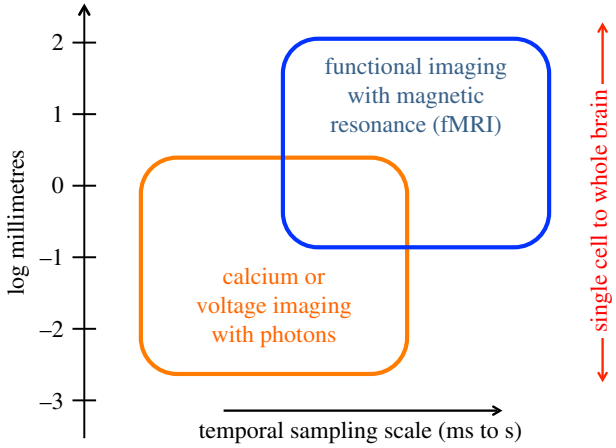

Figure 12. Schematic diagram of the approximate spatial and temporal scales of measurements for multi-photon imaging with calcium and voltage reporters and fMRI, showing that, with impending technological advances, one can aim to overlap these two methods so that it will be possible to perform recordings of activity of each individual neuron in an computational ensemble (e.g. in a cortical column) in an animal model while fMRI can detect the activity at the level of the same ensemble but over the entire animal or human brain (i.e. cover the entire brain at the sub-columnar spatial resolution sufficient to obtain images of the columnar activity).

Competing interests. I declare I have no competing interests.

Funding. The work from CMRR reviewed here was supported by NIH grant P41 EB015894 (NIBIB) (previously P41 RR008079 (NCRR)) and NINDS Institutional Center Core Grants to Support Neuroscience Research (P30 NS076408), and the Human Connectome Project (1U54MH091657) supported by the 16 Institutes and Centers of the National Institutes of Health that support the NIH Blueprint for Neuroscience Research.

Acknowledgements. The author thanks Professor Kâmil Uludağ for generating figures 5 and 6 from our previously published paper.

References

1. Kwong KK *et al.* 1992 Dynamic magnetic resonance imaging of human brain activity during primary sensory stimulation. *Proc. Natl Acad. Sci. USA* **89**, 5675–5679. (doi:10.1073/pnas.89.12.5675)
2. Ogawa S, Tank DW, Menon R, Ellermann JM, Kim SG, Merkle H, Ugurbil K. 1992 Intrinsic signal changes accompanying sensory stimulation: functional brain mapping with magnetic resonance imaging. *Proc. Natl Acad. Sci. USA* **89**, 5951–5955. (doi:10.1073/pnas.89.13.5951)
3. Eklund A, Nichols TE, Knutsson H. 2016 Cluster failure: why fMRI inferences for spatial extent have inflated false-positive rates. *Proc. Natl Acad. Sci. USA* **113**, 7900–7905. (doi:10.1073/pnas.1602413113)
4. Turner R, Grinvald A. 1994 Direct visualization of patterns of deoxyhemoglobin and reoxygenation in monkey cortical vasculature during functional brain activation. *Proc. Soc. Magn. Reson.* **1**, 430.
5. Malonek D, Grinvald A. 1996 Interactions between electrical activity and cortical microcirculation revealed by imaging spectroscopy: implications for functional brain mapping. *Science* **272**, 551–554. (doi:10.1126/science.272.5261.551)
6. Duong TQ, Kim DS, Ugurbil K, Kim SG. 2001 Localized cerebral blood flow response at submillimeter columnar resolution. *Proc. Natl Acad. Sci. USA* **98**, 10 904–10 909. (doi:10.1073/pnas.191101098)
7. O'Herron P, Chhatbar PY, Levy M, Shen Z, Schramm AE, Lu Z, Kara P. 2016 Neural correlates of single-vessel haemodynamic responses *in vivo*. *Nature* **534**, 378–382. (doi:10.1038/nature17965)
8. Pawlik G, Rackl A, Bing RJ. 1981 Quantitative capillary topography and blood flow in the cerebral cortex of cats: an *in vivo* microscopic study. *Brain Res.* **208**, 35–58. (doi:10.1016/0006-8993(81) 90619-3)
9. Tsekos NV, Zhang F, Merkle H, Nagayama M, Iadecola C, Kim SG. 1998 Quantitative measurements of cerebral blood flow in rats using the FAIR technique: correlation with previous iodoantipyrine autoradiographic studies. *Magn. Reson. Med.* **39**, 564–573. (doi:10.1002/mrm.1910390409)
10. Grinvald A, Lieke E, Frostig RD, Gilbert CD, Wiesel TN. 1986 Functional architecture of cortex revealed by optical imaging of intrinsic signals. *Nature* **324**, 361–364. (doi:10.1038/324361a0)
11. Vanzetta I, Slovin H, Omer DB, Grinvald A. 2004 Columnar resolution of blood volume and oximetry functional maps in the behaving monkey; implications for FMRI. *Neuron* **42**, 843–854. (doi:10.1016/j.neuron.2004.04.004)
12. Vanzetta I, Grinvald A. 1999 Increased cortical oxidative metabolism due to sensory stimulation: implications for functional brain imaging. *Science* **286**, 1555–1558. (doi:10.1126/science.286.5444.1555)
13. Sirotin YB, Hillman EM, Bordier C, Das A. 2009 Spatiotemporal precision and hemodynamic mechanism of optical point spreads in alert primates. *Proc. Natl Acad. Sci. USA* **106**, 18 390–18 395. (doi:10.1073/pnas.0905509106)
14. Uludag K, Muller-Bierl B, Ugurbil K. 2009 An integrative model for neuronal activity-induced signal changes for gradient and spin echo functional imaging. *Neuroimage* **48**, 150–165. (doi:10.1016/j.neuroimage.2009.05.051)
15. Segebarth C, Belle V, Delon C, Massarelli R, Decety J, Le Bas JF, Decorps M, Benabid AL. 1994 Functional MRI of the human brain: predominance of signals from extracerebral veins. *Neuroreport* **5**, 813–816. (doi:10.1097/00001756-199403000-00019)
16. Ogawa S, Lee T-M, Kay AR, Tank DW. 1990 Brain magnetic resonance imaging with contrast dependent on blood oxygenation. *Proc. Natl Acad. Sci. USA* **87**, 9868–9872. (doi:10.1073/pnas.87.24.9868)
17. Ogawa S, Lee TM, Nayak AS, Glynn P. 1990 Oxygenation-sensitive contrast in magnetic resonance image of rodent brain at high magnetic fields. *Magn. Reson. Med.* **14**, 68–78. (doi:10.1002/mrm.1910140108)
18. Hoge RD, Atkinson J, Gill B, Crelier GR, Marrett S, Pike GB. 1999 Linear coupling between cerebral blood flow and oxygen consumption in activated human cortex. *Proc. Natl Acad. Sci. USA* **96**, 9403–9408. (doi:10.1073/pnas.96.16.9403)
19. Menon RS, Ogawa S, Tank DW, Ugurbil K. 1993 4 Tesla gradient recalled echo characteristics of photic stimulation-induced signal changes in the human primary visual cortex. *Magn. Reson. Med.* **30**, 380–386. (doi:10.1002/mrm.1910300317)
20. Lai S *et al.* 1993 Identification of vascular structures as a major source of signal contrast in high resolution 2D and 3D functional activation imaging of the motor cortex at 1.5T: preliminary results. *Magn. Reson. Med.* **30**, 387–392. (doi:10.1002/mrm.1910300318)
21. Kim SG, Hendrich K, Hu X, Merkle H, Ugurbil K. 1994 Potential pitfalls of functional MRI using conventional gradient-recalled echo techniques. *NMR Biomed.* **7**, 69–74. (doi:10.1002/nbm.1940070111)
22. Haacke EM *et al.* 1994 2D and 3D high resolution gradient echo functional imaging of the brain: venous contributions to signal in motor cortex studies [published erratum appears in NMR Biomed 1994 Dec;7(8):374]. *NMR Biomed.* **7**, 54–62. (doi:10.1002/nbm.1940070109)
23. Turner R. 2002 How much cortex can a vein drain? Downstream dilution of activation-related cerebral blood oxygenation changes. *Neuroimage* **16**, 1062–1067. (doi:10.1006/nimg.2002.1082)
24. Engel SA, Glover GH, Wandell BA. 1997 Retinotopic organization in human visual cortex and the spatial precision of functional MRI. *Cereb. Cortex* **7**, 181–192. (doi:10.1093/cercor/7.2.181)
25. Parkes LM, Schwarzbach JV, Bouts AA, Deckers RH, Pullens P, Kerskens CM, Norris DG. 2005 Quantifying the spatial resolution of the gradient echo and spin echo BOLD response at 3 Tesla. *Magn. Reson. Med.* **54**, 1465–1472. (doi:10.1002/mrm.20712)
26. Ogawa S, Menon RS, Tank DW, Kim SG, Merkle H, Ellermann JM, Ugurbil K. 1993 Functional brain mapping by blood oxygenation level-dependent contrast magnetic resonance imaging. A comparison of signal characteristics with a biophysical model. *Biophys. J.* **64**, 803–812. (doi:10.1016/S0006-3495(93)81441-3)
27. Yacoub E, Van De Moortele PF, Shmuel A, Ugurbil K. 2005 Signal and noise characteristics of Hahn SE and GE BOLD fMRI at 7T in humans. *Neuroimage* **24**, 738–750. (doi:10.1016/j.neuroimage.2004.09.002)
28. Uludag K, Ugurbil K. 2015 Physiology and physics of the fMRI signal. In *fMRI: from nuclear spins to brain function* (eds K Uludag, K Ugurbil, L Berliner), pp. 163–214. New York, NY: Springer.
29. Duong TQ, Yacoub E, Adriany G, Hu X, Ugurbil K, Kim SG. 2003 Microvascular BOLD contribution at 4 and 7T in the human brain: gradient-echo and spin-echo fMRI with suppression of blood effects. *Magn. Reson. Med.* **49**, 1019–1027. (doi:10.1002/mrm.10472)
30. Oja JM, Gillen J, Kauppinen RA, Kraut M, van Zijl PC. 1999 Venous blood effects in spin-echo fMRI of human brain. *Magn. Reson. Med.* **42**, 617–626. (doi:10.1002/(SICI)1522-2594(199910)42:4<617::AID-MRM1>3.0.CO;2-Q)
31. Lee SP, Silva AC, Ugurbil K, Kim SG. 1999 Diffusion-weighted spin-echo fMRI at 9.4 T: microvascular/tissue contribution to BOLD signal changes. *Magn. Reson. Med.* **42**, 919–928. (doi:10.1002/(SICI)1522-2594(199911)42:5<919::AID-MRM12>3.0.CO;2-8)
32. Boxerman JL, Hamberg LM, Rosen BR, Weisskoff RM. 1995 MR contrast due to intravscular magnetic susceptiblity perturbations. *Magn. Reson. Med.* **34**, 555–556. (doi:10.1002/mrm.1910340412)
33. Jochimsen TH, Norris DG, Mildner T, Moller HE. 2004 Quantifying the intra- and extravascular contributions to spin-echo fMRI at 3T. *Magn. Reson. Med.* **52**, 724–732. (doi:10.1002/mrm.20221)
34. Yacoub E, Duong TQ, Van De Moortele PF, Lindquist M, Adriany G, Kim SG, Ugurbil K, Hu X. 2003 Spin-echo fMRI in humans using high spatial resolutions and high magnetic fields. *Magn. Reson. Med.* **49**, 655–664. (doi:10.1002/mrm.10433)

35. Goense JB, Logothetis NK. 2006 Laminar specificity in monkey V1 using high-resolution SE-fMRI. *Magn. Reson. Imaging* **24**, 381–392. (doi:10.1016/j.mri.2005.12.032)
36. Polimeni JR, Fischl B, Greve DN, Wald LL. 2010 Laminar analysis of 7T BOLD using an imposed spatial activation pattern in human V1. *Neuroimage* **52**, 1334–1346. (doi:10.1016/j.neuroimage.2010.05.005)
37. Nasr S, Polimeni JR, Tootell RB. 2016 Interdigitated color- and disparity-selective columns within human visual cortical areas V2 and V3. *J. Neurosci.* **36**, 1841–1857. (doi:10.1523/JNEUROSCI.3518-15.2016)
38. Muckli L, De Martino F, Vizioli L, Petro LS, Smith FW, Ugurbil K, Goebel R, Yacoub E. 2015 Contextual feedback to superficial layers of V1. *Curr. Biol.* **25**, 2690–2695. (doi:10.1016/j.cub.2015.08.057)
39. De Martino F, Zimmermann J, Adriany G, van de Moortele P-F, Feinberg D, Ugurbil K, Goebel R, Yacoub E. 2011 Evidence towards columnar organization of human area MT with sub-millimetric, 3D, T2 weighted BOLD FMRI at 7 Tesla. *Proc. Int. Soc. Mag. Reson. Med.* **19**, 9.
40. De Martino F, Moerel M, Ugurbil K, Goebel R, Yacoub E, Formisano E. 2015 Frequency preference and attention effects across cortical depths in the human primary auditory cortex. *Proc. Natl Acad. Sci. USA* **112**, 16 036–16 041. (doi:10.1073/pnas.1507552112)
41. Hu X, Yacoub E. 2012 The story of the initial dip in fMRI. *Neuroimage* **62**, 1103–1108. (doi:10.1016/j.neuroimage.2012.03.005)
42. Drew PJ, Shih AY, Kleinfeld D. 2011 Fluctuating and sensory-induced vasodynamics in rodent cortex extend arteriole capacity. *Proc. Natl Acad. Sci. USA* **108**, 8473–8478. (doi:10.1073/pnas.1100428108)
43. Hall CN *et al.* 2014 Capillary pericytes regulate cerebral blood flow in health and disease. *Nature* **508**, 55–60. (doi:10.1038/nature13165)
44. Hill RA, Tong L, Yuan P, Murikinati S, Gupta S, Grutzendler J. 2015 Regional blood flow in the normal and ischemic brain is controlled by arteriolar smooth muscle cell contractility and not by capillary pericytes. *Neuron* **87**, 95–110. (doi:10.1016/j.neuron.2015.06.001)
45. Hillman EM, Devor A, Bouchard MB, Dunn AK, Krauss GW, Skoch J, Bacskai BJ, Dale AM, Boas DA. 2007 Depth-resolved optical imaging and microscopy of vascular compartment dynamics during somatosensory stimulation. *Neuroimage* **35**, 89–104. (doi:10.1016/j.neuroimage.2006.11.032)
46. Gagnon L *et al.* 2015 Quantifying the microvascular origin of BOLD-fMRI from first principles with two-photon microscopy and an oxygen-sensitive nanoprobe. *J. Neurosci.* **35**, 3663–3675. (doi:10.1523/JNEUROSCI.3555-14.2015)
47. Triantafyllou C, Hoge RD, Wald LL. 2006 Effect of spatial smoothing on physiological noise in high-resolution fMRI. *Neuroimage* **32**, 551–557. (doi:10.1016/j.neuroimage.2006.04.182)
48. Triantafyllou C, Hoge RD, Krueger G, Wiggins CJ, Potthast A, Wiggins GC, Wald LL. 2005 Comparison of physiological noise at 1.5T, 3T and 7T and optimization of fMRI acquisition parameters. *Neuroimage* **26**, 243–250. (doi:10.1016/j.neuroimage.2005.01.007)
49. Kruger G, Glover GH. 2001 Physiological noise in oxygenation-sensitive magnetic resonance imaging. *Magn. Reson. Med.* **46**, 631–637. (doi:10.1002/mrm.1240)
50. Hyde JS, Biswal BB, Jesmanowicz A. 2001 High-resolution fMRI using multislice partial k-space GR-EPI with cubic voxels. *Magn. Reson. Med.* **46**, 114–125. (doi:10.1002/mrm.1166)
51. Vaughan JT *et al.* 2001 7T vs. 4T: RF power, homogeneity, and signal-to-noise comparison in head images. *Magn. Reson. Med.* **46**, 24–30. (doi:10.1002/mrm.1156)
52. Tkac I, Oz G, Adriany G, Ugurbil K, Gruetter R. 2009 *In vivo* 1H NMR spectroscopy of the human brain at high magnetic fields: metabolite quantification at 4T vs. 7T. *Magn. Reson. Med.* **62**, 868–879. (doi:10.1002/mrm.22086)
53. Pohmann R, Speck O, Scheffler K. 2015 Signal-to-noise ratio and MR tissue parameters in human brain imaging at 3, 7, and 9.4 tesla using current receive coil arrays. *Magn. Reson. Med.* **75**, 801–809.(doi:10.1002/mrm.25677)
54. Yacoub E *et al.* 2001 Imaging brain function in humans at 7 Tesla. *Magn. Reson. Med.* **45**, 588–594. (doi:10.1002/mrm.1080)
55. Ugurbil K. 2012 The road to functional imaging and ultrahigh fields. *Neuroimage* **62**, 726–735. (doi:10.1016/j.neuroimage.2012.01.134)
56. Yacoub E, Harel N, Ugurbil K. 2008 High-field fMRI unveils orientation columns in humans. *Proc. Natl Acad. Sci. USA* **105**, 10 607–10 612. (doi:10.1073/pnas.0804110105)
57. Cheng K, Waggoner RA, Tanaka K. 2001 Human ocular dominance columns as revealed by high-field functional magnetic resonance imaging. *Neuron* **32**, 359–374. (doi:10.1016/S0896-6273(01)00477-9)
58. Yacoub E, Shmuel A, Logothetis N, Ugurbil K. 2007 Robust detection of ocular dominance columns in humans using Hahn spin echo BOLD functional MRI at 7 Tesla. *Neuroimage* **37**, 1161–1177. (doi:10.1016/j.neuroimage.2007.05.020)
59. Zimmermann J *et al.* 2011 Mapping the organization of axis of motion selective features in human area MT using high-field fMRI. *PLoS ONE* **6**, e28716. (doi:10.1371/journal.pone.0028716)
60. Koopmans PJ, Barth M, Orzada S, Norris DG. 2011 Multi-echo fMRI of the cortical laminae in humans at 7T. *Neuroimage* **56**, 1276–1285. (doi:10.1016/j.neuroimage.2011.02.042)
61. Siero JC, Petridou N, Hoogduin H, Luijten PR, Ramsey NF. 2011 Cortical depth-dependent temporal dynamics of the BOLD response in the human brain. *J. Cereb. Blood Flow Metab.* **31**, 1999–2008. (doi:10.1038/jcbfm.2011.57)
62. De Martino F, Zimmermann J, Muckli L, Ugurbil K, Yacoub E, Goebel R. 2013 Cortical depth dependent functional responses in humans at 7T: improved specificity with 3D GRASE. *PLoS ONE* **8**, e60514. (doi:10.1371/journal.pone.0060514)
63. Olman CA, Harel N, Feinberg DA, He S, Zhang P, Ugurbil K, Yacoub E. 2012 Layer-specific fMRI reflects different neuronal computations at different depths in human V1. *PLoS ONE* **7**, e32536. (doi:10.1371/journal.pone.0032536)
64. Stringer EA, Chen LM, Friedman RM, Gatenby C, Gore JC. 2011 Differentiation of somatosensory cortices by high-resolution fMRI at 7T. *Neuroimage* **54**, 1012–1020. (doi:10.1016/j.neuroimage.2010.09.058)
65. Sanchez-Panchuelo RM, Francis S, Bowtell R, Schluppeck D. 2010 Mapping human somatosensory cortex in individual subjects with 7 T functional MRI. *J. Neurophysiol.* **103**, 2544–2556. (doi:10.1152/jn.01017.2009)
66. Siero JC, Hermes D, Hoogduin H, Luijten PR, Ramsey NF, Petridou N. 2014 BOLD matches neuronal activity at the mm scale: a combined 7T fMRI and ECoG study in human sensorimotor cortex. *Neuroimage* **101**, 177–184. (doi:10.1016/j.neuroimage.2014.07.002)
67. Moerel M, De Martino F, Ugurbil K, Yacoub E, Formisano E. 2015 Processing of frequency and location in human subcortical auditory structures. *Sci. Rep.* **5**, 17048. (doi:10.1038/srep17048)
68. De Martino F, Moerel M, van de Moortele PF, Ugurbil K, Goebel R, Yacoub E, Formisano E. 2013 Spatial organization of frequency preference and selectivity in the human inferior colliculus. *Nat. Commun.* **4**, 1386. (doi:10.1038/ncomms2379)
69. Ugurbil K, Toth L, Kim DS. 2003 How accurate is magnetic resonance imaging of brain function? *Trends Neurosci*. **26**, 108–114. (doi:10.1016/S0166-2236(02)00039-5)
70. Ugurbil K *et al.* 2003 Ultrahigh field magnetic resonance imaging and spectroscopy. *Magn. Reson. Imaging* **21**, 1263–1281. (doi:10.1016/j.mri.2003.08.027)
71. Logothetis NK. 2008 What we can do and what we cannot do with fMRI. *Nature* **453**, 869–878. (10.1038/nature06976)
72. Ugurbil K. 2014 Magnetic resonance imaging at ultrahigh fields. *IEEE Trans. Biomed. Eng.* **61**, 1364–1379. (doi:10.1109/TBME.2014.2313619)
73. Duyn JH. 2012 The future of ultra-high field MRI and fMRI for study of the human brain. *Neuroimage* **62**, 1241–1248. (doi:10.1016/j.neuroimage.2011.10.065)
74. Harel N, Uludag K, Yacoub E, Ugurbil K. 2012 Functional MRI (fMRI) techniques: modern developments. In *Encyclopedia of magnetic resonance* (eds RK Harris, RE Wasylishen). Chichester, UK: John Wiley & Sons.
75. Harel N, Bolan PJ, Turner R, Ugurbil K, Yacoub E. 2010 Recent advances in high-resolution MR application and its implications for neurovascular coupling research. *Front. Neuroenerg.* **2**, 130. (doi:10.3389/fnene.2010.00130)
76. Harel N, Ugurbil K, Uludag K, Yacoub E. 2006 Frontiers of brain mapping using MRI. *J. Magn. Reson. Imaging* **23**, 945–957. (doi:10.1002/jmri.20576)
77. Yacoub E, Shmuel A, Harel N. 2015 High resolution fMRI. In *fMRI: from nuclear spins to brain function* (eds K Uludag, K Ugurbil, L Berliner), pp. 769–793. New York, NY: Springer.
78. Formisano E, Kim DS, Di Salle F, van de Moortele PF, Ugurbil K, Goebel R. 2003 Mirror-symmetric

tonotopic maps in human primary auditory cortex. *Neuron* **40**, 859–869. (doi:10.1016/S0896-6273(03)00669-X)

79. Kay KN, Naselaris T, Prenger RJ, Gallant JL. 2008 Identifying natural images from human brain activity. *Nature* **452**, 352–355. (doi:10.1038/nature06713)
80. Naselaris T, Kay KN, Nishimoto S, Gallant JL. 2011 Encoding and decoding in fMRI. *Neuroimage* **56**, 400–410. (doi:10.1016/j.neuroimage.2010.07.073)
81. Santoro R, Moerel M, De Martino F, Goebel R, Ugurbil K, Yacoub E, Formisano E. 2014 Encoding of natural sounds at multiple spectral and temporal resolutions in the human auditory cortex. *PLoS Comput. Biol.* **10**, e1003412. (doi:10.1371/journal.pcbi.1003412)
82. Naselaris T, Olman CA, Stansbury DE, Ugurbil K, Gallant JL. 2015 A voxel-wise encoding model for early visual areas decodes mental images of remembered scenes. *Neuroimage* **105**, 215–228. (doi:10.1016/j.neuroimage.2014.10.018)
83. Menon RS. 2002 Postacquisition suppression of large-vessel BOLD signals in high-resolution fMRI. *Magn. Reson. Med.* **47**, 1–9. (doi:10.1002/mrm.10041)
84. Shmuel A, Maier A. 2015 Locally measured neuronal correlates of functional MRI signals. In *fMRI: from nuclear spins to brain function* (eds K Uludag, K Ugurbil, L Berliner), pp. 105–128. New York, NY: Springer.
85. Shmuel A, Yacoub E, Pfeuffer J, Van de Moortele PF, Adriany G, Hu X, Ugurbil K. 2002 Sustained negative BOLD, blood flow and oxygen consumption response and its coupling to the positive response in the human brain. *Neuron* **36**, 1195–1210. (doi:10.1016/S0896-6273(02)01061-9)
86. Shmuel A, Augath M, Oeltermann A, Logothetis NK. 2006 Negative functional MRI response correlates with decreases in neuronal activity in monkey visual area V1. *Nat. Neurosci.* **9**, 569–577. (doi:10.1038/nn1675)
87. Gourtzelidis P, Tzagarakis C, Lewis SM, Crowe DA, Auerbach E, Jerde TA, Ugurbil K, Georgopoulos AP. 2005 Mental maze solving: directional fMRI tuning and population coding in the superior parietal lobule. *Exp. Brain Res.* **165**, 273–282. (doi:10.1007/s00221-005-2298-6)
88. Jerde TA *et al.* 2008 Ultra-high field parallel imaging of the superior parietal lobule during mental maze solving. *Exp. Brain Res.* **187**, 551–561. (doi:10.1007/s00221-008-1318-8)
89. Crowe DA, Chafee MV, Averbeck BB, Georgopoulos AP. 2004 Neural activity in primate parietal area 7a related to spatial analysis of visual mazes. *Cereb. Cortex* **14**, 23–34. (doi:10.1093/cercor/bhg088)
90. Biswal B, Yetkin FZ, Haughton VM, Hyde JS. 1995 Functional connectivity in the motor cortex of resting human brain using echo-planar MRI. *Magn. Reson. Med.* **34**, 537–541. (doi:10.1002/mrm.1910340409)
91. Fox MD, Raichle ME. 2007 Spontaneous fluctuations in brain activity observed with functional magnetic resonance imaging. *Nat. Rev. Neurosci.* **8**, 700–711. (doi:10.1038/nrn2201)
92. Vincent JL *et al.* 2007 Intrinsic functional architecture in the anaesthetized monkey brain. *Nature* **447**, 83–86. (doi:10.1038/nature05758)
93. Beckmann CF, DeLuca M, Devlin JT, Smith SM. 2005 Investigations into resting-state connectivity using independent component analysis. *Phil. Trans. R Soc. B* **360**, 1001–1013. (doi:10.1098/rstb.2005.1634)
94. Smith SM, Miller KL, Salimi-Khorshidi G, Webster M, Beckmann CF, Nichols TE, Ramsey JD, Woolrich MW. 2011 Network modelling methods for FMRI. *Neuroimage* **54**, 875–891. (doi:10.1016/j.neuroimage.2010.08.063)
95. Smith SM *et al.* 2009 Correspondence of the brain's functional architecture during activation and rest. *Proc. Natl Acad. Sci. USA* **106**, 13 040–13 045. (doi:10.1073/pnas.0905267106)
96. Greicius MD, Krasnow B, Reiss AL, Menon V. 2003 Functional connectivity in the resting brain: a network analysis of the default mode hypothesis. *Proc. Natl Acad. Sci. USA* **100**, 253–258. (doi:10.1073/pnas.0135058100)
97. Smith SM *et al.* 2013 Functional connectomics from resting-state fMRI. *Trends Cogn. Sci.* **17**, 666–682. (doi:10.1016/j.tics.2013.09.016)
98. Smith SM *et al.* 2013 Resting-state fMRI in the Human Connectome Project. *Neuroimage* **80**, 144–168. (doi:10.1016/j.neuroimage.2013.05.039)
99. Ugurbil K *et al.* 2013 Pushing spatial and temporal resolution for functional and diffusion MRI in the Human Connectome Project. *Neuroimage* **80**, 80–104. (doi:10.1016/j.neuroimage.2013.05.012)
100. Griffanti L *et al.* 2014 ICA-based artefact removal and accelerated fMRI acquisition for improved resting state network imaging. *Neuroimage* **95**, 232–247. (doi:10.1016/j.neuroimage.2014.03.034)
101. Feinberg DA *et al.* 2010 Multiplexed echo planar imaging for sub-second whole brain FMRI and fast diffusion imaging. *PLoS ONE* **5**, e15710. (doi:10.1371/journal.pone.0015710)
102. Mitra PP, Ogawa S, Hu X, Ugurbil K. 1997 The nature of spatiotemporal changes in cerebral hemodynamics as manifested in functional magnetic resonance imaging. *Magn. Reson. Med.* **37**, 511–518. (doi:10.1002/mrm.1910370407)
103. Shmueli K, van Gelderen P, de Zwart JA, Horovitz SG, Fukunaga M, Jansma JM, Duyn JH. 2007 Low-frequency fluctuations in the cardiac rate as a source of variance in the resting-state fMRI BOLD signal. *Neuroimage* **38**, 306–320. (10.1016/j.neuroimage.2007.07.037)
104. Van Essen DC, Smith SM, Barch DM, Behrens TE, Yacoub E, Ugurbil K, for the WU-Minn HCP Consortium. 2013 The WU-Minn Human Connectome Project: an overview. *Neuroimage* **80**, 62–79. (doi:10.1016/j.neuroimage.2013.05.041)
105. Kenet T, Bibitchkov D, Tsodyks M, Grinvald A, Arieli A. 2003 Spontaneously emerging cortical representations of visual attributes. *Nature* **425**, 954–956. (doi:10.1038/nature02078)
106. Shmuel A, Leopold DA. 2008 Neuronal correlates of spontaneous fluctuations in fMRI signals in monkey visual cortex: implications for functional connectivity at rest. *Hum. Brain Mapp.* **29**, 751–761. (doi:10.1002/hbm.20580)
107. He BJ, Snyder AZ, Zempel JM, Smyth MD, Raichle ME. 2008 Electrophysiological correlates of the brain's intrinsic large-scale functional architecture. *Proc. Natl. Acad. Sci. USA* **105**, 16 039–16 044. (doi:10.1073/pnas.0807010105)
108. Liu Z, Fukunaga M, de Zwart JA, Duyn JH. 2010 Large-scale spontaneous fluctuations and correlations in brain electrical activity observed with magnetoencephalography. *Neuroimage* **51**, 102–111. (doi:10.1016/j.neuroimage.2010.01.092)
109. Leopold DA, Maier A. 2012 Ongoing physiological processes in the cerebral cortex. *Neuroimage* **62**, 2190–2200. (doi:10.1016/j.neuroimage.2011.10.059)
110. Liu X, Zhu XH, Zhang Y, Chen W. 2011 Neural origin of spontaneous hemodynamic fluctuations in rats under burst-suppression anesthesia condition. *Cereb. Cortex* **21**, 374–384. (doi:10.1093/cercor/bhq105)
111. Scholvinck ML, Maier A, Ye FQ, Duyn JH, Leopold DA. 2010 Neural basis of global resting-state fMRI activity. *Proc. Natl Acad. Sci. USA* **107**, 10 238–10 243. (doi:10.1073/pnas.0913110107)
112. Scholvinck ML, Leopold DA, Brookes MJ, Khader PH. 2013 The contribution of electrophysiology to functional connectivity mapping. *Neuroimage* **80**, 297–306. (doi:10.1016/j.neuroimage.2013.04.010)
113. Liu X, Yanagawa T, Leopold DA, Fujii N, Duyn JH. 2015 Robust long-range coordination of spontaneous neural activity in waking, sleep and anesthesia. *Cereb. Cortex* **25**, 2929–2938. (doi:10.1093/cercor/bhu089)
114. Tavor I, Parker Jones O, Mars RB, Smith SM, Behrens TE, Jbabdi S. 2016 Task-free MRI predicts individual differences in brain activity during task performance. *Science* **352**, 216–220. (doi:10.1126/science.aad8127)
115. Smith SM *et al.* 2015 A positive-negative mode of population covariation links brain connectivity, demographics and behavior. *Nat. Neurosci.* **18**, 1565–1567. (doi:10.1038/nn.4125)
116. Finn ES, Shen X, Scheinost D, Rosenberg MD, Huang J, Chun MM, Papademetris X, Constable RT. 2015 Functional connectome fingerprinting: identifying individuals using patterns of brain connectivity. *Nat. Neurosci.* **18**, 1664–1671. (doi:10.1038/nn.4135)
117. Hawrylycz M *et al.* 2015 Canonical genetic signatures of the adult human brain. *Nat. Neurosci.* **18**, 1832–1844. (doi:10.1038/nn.4171)
118. Vu AT, Auerbach E, Lenglet C, Moeller S, Sotiropoulos SN, Jbabdi S, Andersson J, Yacoub E, Ugurbil K. 2015 High resolution whole brain diffusion imaging at 7T for the Human Connectome Project. *Neuroimage* **122**, 318–331. (doi:10.1016/j.neuroimage.2015.08.004)
119. Sotiropoulos SN *et al.* 2016 Fusion in diffusion MRI for improved fibre orientation estimation: an application to the 3T and 7T data of the Human Connectome Project. *Neuroimage* **134**, 396–409. (doi:10.1016/j.neuroimage.2016.04.014)